

1 **Development of a copper-graphene nanocomposite based transparent**

2 **coating with antiviral activity against influenza virus**

3

4 Indrani Das Jana^{1#}, Partha Kumbhakar^{2#}, Saptarshi Banerjee¹, Chinmayee Chowde Gowda³, Nandita
5 Kedia¹, Saikat Kumar Kuila², Sushanta Banerjee⁴, Narayan Chandra Das⁵, Amit Kumar Das¹, Indranil
6 Manna², Chandra Sekhar Tiwary^{2*}, Arindam Mondal^{1*}

7

8 ¹School of Bioscience, Indian Institute of Technology Kharagpur, India

9 ²Department of Metallurgical and Materials Engineering, Indian Institute of Technology Kharagpur, India

10 ³School of Nanoscience and Technology, Indian Institute of Technology Kharagpur, India

11 ⁴Material Science Center, Indian Institute of Technology Kharagpur, India

12 ⁵Rubber Technology Center, Indian Institute of Technology Kharagpur, India

13 # Authors contributed equally

14

15 * Address for correspondence: arindam.mondal@iitkgp.ac.in, chandra.tiwary@metal.iitkgp.ac.in

16

17 Keywords: Nanocomposite, Influenza virus, Nano-Luciferase, Antivirals coating

18

19

20 **Abstract**

21 Respiratory infections by RNA viruses are one of the major burdens upon global health and economy.
22 Viruses like influenza or coronaviruses can be transmitted through respiratory droplets or contaminated
23 surfaces. An effective antiviral coating can decrease the viability of the virus particles in the outside
24 environment significantly, hence reducing their transmission rate. In this work, we have screened a series
25 of nanoparticles and their composites for antiviral activity using Nano Luciferase based highly sensitive
26 influenza A reporter virus. Using this screening system, we have identified copper-graphene (Cu-Gr)
27 nanocomposite shows strong antiviral activity. Extensive material and biological characterization of the
28 nanocomposite suggested a unique metal oxide embedded graphene sheet architecture that can inactivate
29 the virion particles only within 30 minutes of pre-incubation and subsequently interferes with the entry of
30 these virion particles into the host cell. This ultimately results in reduced viral gene expression, replication
31 and production of progeny virus particles, slowing down the overall pace of progression of infection. Using
32 PVA as a capping agent, we have been able to generate a Cu-Gr nanocomposite based highly transparent
33 coating that retains its original antiviral activity in the solid form.

34

35

36 **Introduction**

37 The emergence of novel virus strains and the associated outbreaks are becoming a significant threat to
38 mankind (Koven 2020). The currently ongoing pandemic, caused by the Severe Acute Respiratory
39 Syndrome- Coronavirus 2 (SARS-CoV-2), has brought the majority of the world to a grinding halt, severely
40 impacting health & economy across the nations (Letko, Marzi, and Munster 2020). So far, the COVID-19
41 pandemic has claimed 720,000 lives resulting from 19.4 million infections globally. This reminds us of the
42 great 1918 Spanish flu pandemic by the influenza virus, which resulted in 500 million infections with 50
43 million deaths (Johnson and Mueller 2002) (Patterson and Pyle 2019) (Taubenberger and Morens 2006)
44 (Landrigan et al. 2018). Till date, there have been four worldwide pandemics caused by influenza viruses
45 in the last century (1918, 1957, 1968, 2009) (World Health Organization 2018) (Saunders-Hastings and
46 Krewski 2016), while Covid19 is the first pandemic caused by the Coronavirus (Y. Wu et al. 2020). Other
47 than pandemics, influenza A and B viruses cause seasonal outbreaks (290,000 to 650,000 deaths worldwide:
48 CDC FLUVIEW] and different coronaviruses cause mild flu-like symptoms to severe respiratory infections
49 (SARS (De Wit et al. 2016) and MERS (Lin et al. 2019) coronavirus epidemics during 2002 and 2012
50 respectively) (Fehr and Perlman 2015). Clearly, recurring respiratory infections caused by these viruses
51 are becoming one of the global human health problem.

52

53 Both influenza and coronaviruses cause respiratory infections, which can be transmitted from infected to
54 healthy individuals through respiratory droplets, aerosols or contacts. These respiratory pathogens are
55 known for their ability to persist on inanimate surfaces for days and even up to months, depending upon
56 weather conditions (Vasickova et al. 2010). As a result, touching contaminated surfaces in public places is
57 a potential route of viral transmission. In fact, the inanimate surfaces have been identified as a major cause
58 of infections, especially in institutions where individuals are in contact with patients or contaminated
59 fomites. Thus, the development of low cost and easily scalable antiviral coating materials, which could be
60 widely applied to various surfaces in order to inactivate the virus particles in the environment, may serve
61 as an effective way to reduce the chance of infection and hence to lower the overall speed of transmission.

62

63 Different metal oxides, including Cu and Ag have been explored for their biocidal activity in soluble as
64 well as in insoluble forms (Minoshima et al. 2016) . Copper and silver nanoparticles have remarkable
65 properties like high electrical and thermal conductivity (Barani et al. 2020; D. Deng et al. 2013), superior
66 catalytic nature (Gawande et al. 2016), anti-fungal (Cioffi et al. 2005) and bacteriostatic activities (Ruparelia
67 et al. 2008) to name a few. Solid-state cuprous oxide and silver nitrate have been shown to inactivate virus
68 particles through interfering with the activity of the surface antigen, hemagglutinin (HA), thereby blocking

69 the attachment of the virus to the host cell receptors (Fehr and Perlman 2015) (Sunada, Minoshima, and
70 Hashimoto 2012). Cuprous oxide nanoparticles had also been shown to inhibit the attachment and entry
71 stages of Hepatitis C Virus infection, hence suggesting a generic mechanism for the copper-based
72 nanoparticles for their antiviral activities (Hang et al. 2015). This may also explain the lesser viability of
73 infectious SARS-CoV-2 particles on copper surfaces (8 h) when compared to stainless steel and plastic
74 surfaces (72 h) (Neeltje van Doremalen et al. 2020). Biological activity of the Cu or Ag nanoparticles largely
75 depends upon their size, shape, stability and capping agent. Due to the high reactivity of these nanoparticles,
76 they can undergo rapid agglomeration leading to the drastic reduction of their activity (Ma et al. 2011). One
77 way to overcome this instability is to form a composite with other organic or inorganic compounds which
78 stabilizes the nanoparticles by altering their surface architecture (Perdikaki et al. 2018).

79

80 Graphene is composed of a single atom thick sheet of sp₂ hybridized carbon atoms that forms a honeycomb
81 lattice (Mohammed et al. 2020; Palmieri and Papi 2020). This structure of graphene is responsible for its
82 large surface area, excellent electrical conductivity, strong mechanical strength and unique physicochemical
83 properties (Edwards and Coleman 2013; Eigler and Hirsch 2014; Novoselov et al. 2012). It is used
84 extensively in the field of nano-medicine due to easy surface functionality and controlled selectivity (Park
85 et al. 2020). In recent times, the two dimensional sheet of graphene has caught much attention due to its
86 antimicrobial and antiviral activity (Georgakilas et al. 2012). Differentially functionalized graphene oxide
87 sheets can warp and encapsulate microorganisms, thereby severely restricting their interaction with host
88 cells (Perdikaki et al. 2018) (Vinothini and Rajan 2017) (Karahan et al. 2018). For example, sulfate
89 functionalized reduced graphene oxide has been shown to interact with the positively charged surface
90 proteins of different orthopoxvirus strains (Ziem et al. 2016) (Ye et al. 2015). In this work, we have
91 performed an extensive investigation of the potential antiviral activity of copper (Cu) nanoparticles, silver
92 (Ag) nanoparticles, graphene (Gr) and their hybrid versions (nanocomposite materials) Ag-graphene, Cu-
93 graphene and Ag-Cu-graphene against respiratory viruses using influenza A virus as a model system. Our
94 data shows that prior incubation with the colloidal Cu-Gr nanocomposite can impose a strong reduction in
95 viral infectivity, which gets manifested in the reduced viral entry, gene expression and subsequent
96 production of progeny virions. Extensive material characterization using UV-Visible absorption and Raman
97 spectroscopy along with X-Ray Diffraction (XRD) reveals a unique architecture of copper oxide decorated
98 two-dimensional graphene sheets. The shape, size and distribution of the hybrid nanoparticles were also
99 studied using Scanning Electron Microscopy (SEM) and Energy-dispersive X-ray spectroscopy (EDAX).
100 Finally, we have developed for the first time a polyvinyl alcohol (PVA) based copper-graphene
101 nanocomposite coating, which is completely transparent and shows strong antiviral activity in the solid
102 phase.

103

104 **Results**

105 **Synthesis and preliminary characterization of the nanoparticles and nanocomposites**

106 We have synthesized various nanoparticles and their hybrids using a simple and cost-effective chemical
107 method as discussed in the experimental section. The synthesized materials are Cu nanoparticles, Ag
108 nanoparticles, graphene (Gr) and their hybrid versions Ag- graphene, Cu- graphene and Ag-Cu-graphene
109 (Figure 1 A, B). Visible absorption spectra of each of these variants confirms the presence of respective
110 components either alone or in combination with their composite partners, as shown in Figure 1C and D. The
111 peak at 418 nm confirms the formation of Ag colloidal nanoparticles (Jin et al. 2005). From literature, it is
112 attributed to Surface Plasmon Resonance with spherical nature (Hu et al. 2013). From the UV-vis spectra
113 of the composite Ag-Gr, Plasmon absorption band at around 410 nm, indicates the formation of a hybrid
114 structure. Incorporation of Ag nanoparticles on graphene sheets had led to a blue shift of the surface
115 plasmon resonance, a characteristic similar to previous reports (Kim et al. 2018).

116 Furthermore, Cu nanoparticles, due to exposure of air at room temperature, goes through surface oxidation,
117 which is the reason that samples contain oxygen in +1 and +2 states forming CuO or Cu₂O (Yao et al.
118 2005). Composite including both Ag and Cu nanoparticles were also analyzed from the absorption
119 spectrum. A broad graphene peak was observed at 280 nm in the composite. Both Ag and Cu nanoparticle
120 plasmon peaks were observed and confirmed the presence of the colloidal nanoparticles on graphene sheets
121 (Darabdhara et al. 2017). Particularly, Figure 1D shows the absorption spectra of the composites and it
122 confirms the formation of graphene and CuO/Cu₂O nanoparticles. An absorption peak at 262 nm is due to
123 $\pi \rightarrow \pi^*$ transition in C=C bond of graphene. Another absorption band at ~350-450 nm is attributed to the
124 intrinsic band to band transition of the CuO and Cu₂O (Zhang et al. 2020). A blue shift was observed in the
125 peak position compared to bulk CuO; this might be due to the quantum confinement effects exhibited by
126 the particle when the size varies from bulk to nano. These UV-Vis peaks were well matched with CuO and
127 Cu₂O absorption profiles from previous studies (Chan et al. 2007). A broadened plasmon resonance peak
128 for Cu-Gr nanocomposites is due to irregular shapes and sizes of the particles (Zhang et al. 2020).

129 **Screening of nanoparticles and their hybrids for antiviral activity**

130 To test the antiviral activity of synthesized nanomaterials and their composites we have used a
131 bioluminescent reporter variant of the influenza A virus, strain A/H1N1/WSN/1933, that has been
132 previously reported by Tran et al. (Tran et al. 2013). This virus has a Nano-Luciferase (NLuc) gene fused
133 to the carboxy-terminal of the viral PA gene, interspaced by the “self-cleaving” 2A peptide encoding

134 sequence from porcine teschovirus. The Nano-Luc-influenza A reporter virus, as a part of its gene
135 expression, synthesizes the PA-2A-NLuc polypeptide, which gets self-cleaved to produce Nano-luciferase.
136 Subsequently, the luciferase activity could be measured as a quantitative estimate of viral gene expression
137 and hence progression of virus replication cycle inside the cells. To test whether the Nano-luciferase activity
138 could actually serve as a proxy to virus replication, we have infected MDCK cells with different amounts
139 of input virus and viral replication/gene expression was monitored using Nano-Glo assay (Promega). As
140 shown in Figure 3A, there is a linear relationship between multiplicity of infection (0.01-0.1) and luciferase
141 light unit measurements ($R^2 = 0.9294$), where an increase in one log in the input virus amount leads to about
142 50% increase in the luciferase activity or vice versa, measured at 8 hours of post-infection. This data
143 suggests that the Nano-luciferase influenza A reporter virus could serve as an excellent tool to study the
144 antiviral activity of various nanoparticles or their nanocomposites used in this study.

145 In order to test the antiviral activity, we have standardized a “Nano-Luc reporter assay” described in Figure
146 3B. Briefly, Nano-luciferase influenza A reporter viruses were pre-incubated with the 5uM colloidal
147 suspensions of each of the nanoparticles/ composites or with the vehicle control for 30 minutes at room
148 temperature and subsequently used to infect MDCK cells at an MOI of 0.1. Luciferase activity was
149 measured at 8 hours of post infection and plotted as a relative percentage of the vehicle control set (Figure
150 3C). Prior treatment of the virus stock solution with Cu-Gr composite showed 64% reduction in viral gene
151 expression, while prior treatment with Ag-Gr resulted in 20% reduction. Treatment with other materials
152 shows no significant decrease in luciferase activity. From the correlation of input virus units and the
153 corresponding luciferase activity, as shown in Figure 3A, it can be inferred that prior treatment with Cu-Gr
154 solution resulted in more than 10-fold reductions in the infectious virus population that has been used to
155 infect the MDCK cells. In this context, it should be noted that none of the materials showed substantial
156 cytotoxicity upon Madin-Darby Canine Kidney cells (MDCK) within the concentration range of 0.5 uM -
157 5.0 uM as evaluated using MTT assay (Figure 2). Hence, the reduction in Nano-luciferase activity as a
158 result of prior exposure to Cu-Gr should be attributed exclusively to the reduction of the infectivity of the
159 Nano-luciferase reporter virus. Henceforth, we focused upon the extensive characterization of the Cu-Gr
160 nanocomposite.

161

162 **Material characterization of Cu-Gr nanocomposite**

163 We have extensively characterized the structural parameters of the synthesized Cu-Gr nanocomposites by
164 optical measurements. Figure 4 A depicts Raman spectra of synthesized Cu-Gr nanocomposite samples at
165 excitation of 532 nm in the range of 200 cm^{-1} to 3000 cm^{-1} . With Raman spectroscopy, we are able to
166 distinguish both pristine graphene and copper peaks. The presence of D peak (1361 cm^{-1}) and G peak (1527

167 cm^{-1}) confirms the existence of graphene in the samples synthesized. Generally, D peak originates from
168 defects in the hexagonal sp^2 carbon system while the G peak arises due to the stretching vibration of sp^2
169 carbon pairs in both rings and chains (Ferrari et al. 2006). Except, D and G peak, the 2D peak arises at
170 $\sim 2700 \text{ cm}^{-1}$. The 2D peak originates due to transverse optical (TO) phonons around the K point and is
171 activated by triple resonance Raman scattering (TRRS) (J. Bin Wu et al. 2018). In the measured Raman
172 spectra (Figure 4B), three peaks are (280 cm^{-1} , 350 cm^{-1} and 654 cm^{-1}) observed to confirm the formation
173 of oxide of Cu and originate due to the first order phonon scattering. The peaks are assigned to A_g and 2B_g
174 peaks of copper oxide (Y. Deng et al. 2016). The graphene sheets are also seen in the optical images, as
175 shown in the inset of Figure 4 A. Figure 4B shows the XRD patterns of graphene, CuO , and Cu_2O
176 nanoparticles, which confirm the crystalline phase of composites samples (standard JCPDS file number 35–
177 0505, 80–1917). Interestingly, the intensity of the Cu_2O is more intense compared to that of the CuO peaks,
178 suggesting a higher abundance of Cu_2O on the surface of the graphene sheets. No diffraction peaks
179 corresponding to impurities are observed in the patterns.

180

181 **Extensive characterization of antiviral property of Colloidal Cu-Gr nanocomposite**

182 Followed by the material characterization, we have invested significant efforts for the characterization of
183 the antiviral property of the Cu-Gr nanocomposites in its colloidal form. First, we have used the Nano-Luc
184 reporter assay in order to identify the optimal time and concentration required for its antiviral activity. The
185 Nano-Luc reporter assay was performed where the influenza A reporter virus was pretreated with the
186 colloidal form of the Cu-Gr nanocomposite for various time periods before using them for infecting MDCK
187 cells. As evidenced from Figure 5A, a sharp decrease ($>50\%$) in the reporter activity was observed as a
188 result of 30 minutes of preincubation with Cu-Gr composite, while longer times of preincubation showed
189 only minor additional reduction. This data suggested that 30 minutes of preincubation with Cu-Gr
190 composite can lead to more than tenfold reduction in input virus titer that ultimately results in $\sim 50\%$
191 decrease in reporter activity. Subsequently, we tried to identify the optimal concentration of the Cu-Gr
192 composite required for its antiviral activity. Different concentrations of the Cu-Gr composite (50nM,
193 100nM, 500nM, 1 μM , 2 μM and 5 μM , respectively) were used to treat the Nano-Luc influenza A reporter
194 virus for 30 minutes followed by performing Nano-Luc reporter assay with the same. A precise dose
195 dependent decrease in reporter activity and hence virus replication was observed as a result of prior
196 treatment with Cu-Gr composite within the concentration range of 0.5mM to 5mM (Figure 5B). While
197 higher concentration (10 μM) further reduced reporter activity, it may also show cytotoxicity upon the cells,
198 hence excluded from the subsequent experiment.

199

200 Next, we intended to test whether the reduction in the luciferase activity of the reporter virus, as a result of
201 pretreatment with Cu-Gr nanocomposite, can also be correlated to the reduction of progeny virus titer. A
202 non-reporter variant of the influenza A/H1N1/WNS/1933 virus was used for this purpose. Virus stock
203 solutions were either treated with two different concentrations of Cu-Gr nanocomposites (1 μ M and 5 μ M)
204 or with the vehicle control prior to infection on MDCK cells. Plaque assay was performed to measure the
205 titer of the progeny virus particles harvested at 8 hours of post-infection. There is about 40% decrease in
206 viral titer for the sets treated 5 μ M Cu-Gr solution with respect to the vehicle treated sets. Treatment with
207 1 μ M Cu-Gr nanocomposite shows non-significant decrease in viral titer. This data further substantiates the
208 fact that treatment with 5 μ M Cu-Gr significantly reduces viral infectivity which results in a decrease in
209 viral gene expression, replication and subsequent production of viral titer (Figure 5C). The plaque assay
210 titer data are tabulated in Figure 5D.

211

212 **Prior treatment with Cu-Gr nanocomposite explicitly inhibits virus entry into the cells**

213 At this point, we sought to examine the molecular mechanism by which Cu-Gr nanocomposite interferes
214 with virus replication cycle. Metal nanoparticles have been shown to interfere with the integrity of the virus
215 particles or the activity of the surface glycoproteins that may interfere with the entry of virus particles into
216 the host cells (Sunada, Minoshima, and Hashimoto 2012) (Ting Du. 2018). Hence, to investigate the effect
217 of pretreatment of Cu-Gr specifically upon virus entry step, we have performed an ‘entry assay’ (Figure
218 6A). The non-reporter variant of Influenza A WSN virus were either treated with Cu-Gr or with solvent
219 and subsequently used to infect MDCK cells in a synchronized fashion. Post entry, cells were incubated
220 with cycloheximide containing media for one hour to allow the import of the incoming viral
221 ribonucleoprotein complexes (RNPs) into the nucleus. Subsequently, the incoming viral RNPs were stained
222 with antibodies specific to viral Nucleoprotein (NP), which is the major component of the RNPs. As shown
223 in the Figure 6 B, input viral RNPs are solely detected inside the nucleus of the infected cells irrespective
224 of the treatment. However, prior exposure to the Cu-Gr composite resulted in a significant reduction in the
225 number of NP positive cells. A quantitative analysis of 5 different fields with a total of 500 cells for both
226 treated and untreated sets shows roughly 80% decrease in number of NP positive cells in the Cu-Gr treated
227 set, with respect to the untreated one (Figure 6C). This data clearly suggests that exposure to Cu-Gr
228 nanocomposite compromises the ability of the virus particles to enter into the host cell, possibly by
229 impacting the structural integrity of the virion particles.

230

231 **Development of a Cu-Gr nanocomposite based transparent coating with strong antiviral activity**

232 The ability of Cu-Gr nanocomposite to reduce the infectivity of influenza A virus prompted us to test its
233 ability to inactivate influenza virus in the solid form. For this purpose, we have coated different wells of a

234 48 well plate with a series of coating solutions containing different concentrations of Cu-Gr composite
235 (1 μ M, 5 μ M, 10 μ M and 20 μ M) and polyvinyl alcohol (PVA) (1mm, 5mm, and 10mm) as a capping agent.
236 As a control, wells were coated with only PVA. This process generated a thin transparent film of Cu-Gr
237 nanocomposite onto the surface of each well. To test the antiviral activity of these films, defined amounts
238 of Nano-Luc influenza A reporter virus were inoculated in these coated wells and incubated for 30 minutes.
239 Post treatment, infectivity of these virus inoculums were tested on MDCK cells using the Nano-Luc reporter
240 assay as mentioned above. Prior exposure to the coating materials having various concentrations of Cu-Gr
241 composite blended in different amounts of PVA resulted in differential effects upon viral replication (Figure
242 7). Films containing different concentrations of Cu-Gr composite, either in absence or in presence 1mM
243 PVA barely showed any impact upon the infectivity of the virus. In contrast, an exact dose-dependent
244 decrease in viral gene expression was observed as a result of prior treatment with the films containing
245 increasing concentrations of Cu-Gr Composite in 5mM PVA. This antiviral activity was even more
246 pronounced (70% decrease in Nano-Luc activity) for the films containing 1-5 μ M of Cu-Gr with 10mM of
247 PVA. Together, this data shows 5 μ M of Cu-Gr composite capped with 10mM of PVA could be used to
248 generate a transparent coating with high antiviral activity.

249 Encouraged by the results mentioned above, we have used dip-coating method used to coat a tempered
250 glass with the Cu-Gr solution with optimum concentration. The glass unit was kept to soak the solution for
251 24 h and then air-dried naturally as shown in (Figure 8A). No formation of visibly aggregated spots or
252 clogging was observed on the glass surface. A clean, transparent screen was obtained, and when fixed on a
253 cell phone, there was no compromisation of light intensity or clarity of image on the display screen observed
254 (Figure 8B). Optical transmittance spectra confirm the transparency of the coating on glass substrates
255 (Figure 8C). As observed from the SEM images (Figure 8D), the Cu-O nanoparticles were uniformly
256 embedded on top of the graphene layer. Elemental analysis of Cu-Gr compounds was conducted by color
257 mapping and EDAX analysis. The data presented in the right panel of Figure 8D and Figure 8E confirmed
258 the presence of C, O, and Cu elements in the composites sample and their uniform distribution in the sample.
259 Figure 8F shows a schematic representation of the Cu₂O and CuO nanoparticles embedded on the graphene
260 sheets with PVA as a binding agent.

261

262 **Discussions**

263 RNA viruses constitute one of the broader families of human pathogens, including influenza, Nipah, Ebola,
264 SARS or MERS-Coronaviruses. Irrespective of their specific differences in virus replication cycle, all of
265 these viruses share broader structural similarities. The viral genomic RNA remains enwrapped with single
266 or multiple viral proteins and remains enclosed within the lipid bilayer envelope embedded with viral spike

267 proteins. The integrity of the lipid envelope and the functionality of the spike proteins are not only crucial
268 for the protection of the viral genomic materials in the outer environment but also indispensable for
269 conducting the first two steps of the virus life cycle that are “attachment” and “entry” (Jane Flint, Vincent
270 R 2015). In this study, we have identified Cu-Gr nanocomposite as a potential antiviral agent that can
271 interfere with these two steps of the influenza A virus life cycle, possibly through compromising the
272 structural integrity of the virion particles.

273 We, for the first time, have used a highly sensitive Nano-Luc reporter assay to perform an unbiased
274 screening of a series of nanoparticles and their composite materials in order to identify a coating substance
275 with strong antiviral activity. Our data identified Cu-Gr nanocomposite as the most potential antiviral agent.
276 Interestingly, Cu nanoparticles or graphene individually showed minimal or no antiviral activity in our
277 assay while a hybrid between these two showed at least ten-fold decrease in effective viral titer. This might
278 be due to the property of the composite substances, which is not just a hybrid between two materials in their
279 original state, but rather a combination of the modified version of the materials (Ramakrishnan et al. 2015).
280 This can also be substantiated from the previous studies showing metal-ion based composites shows better
281 activity compared to that of metal nanoparticles itself (Minoshima et al. 2016; Perdikaki et al. 2018; Sunada,
282 Minoshima, and Hashimoto 2012). Studies also reveal that the antiviral activity mainly depends on the
283 presence of ions generated from the surface of nanoparticles (Ma et al. 2011) (Shen et al. 2010). Our XRD
284 data clearly indicates the presence of various copper oxide species, Cu₂O and CuO, embedded in the
285 graphene sheets which may serve as the basis for the antiviral activity of the composite material. The
286 presence of reactive oxygen species in Cu_xO-graphene sheets may provide ions, which may interfere with
287 the structural integrity of the lipid bilayer membrane or the surface antigens of the virion particles. This
288 interference should compromise the ability of the virus particles to interact with the cell surface receptor
289 essential for the attachment and subsequent entry into the host cell. Our entry assay supports this hypothesis,
290 as prior treatment with Cu-Gr composite resulted in significant reduction in the percentage of infection
291 positive cells with respect to the vehicle treated set.

292 Finally, we have used PVA as a capping agent and identified optimum concentrations of Cu-Gr and PVA
293 to develop a thin transparent coating with intense antiviral activity. While we have used dip-coating method
294 to coat a tempered glass with high visibility, other forms of coatings like doctor’s blade technique, spin
295 coating, and spray coating can also be implemented. Due to the high transmission efficiency, such coating
296 material could be implemented on a wide variety of surfaces, which could radically decrease the stability
297 of the virus particles in the outer environment and hence reduce the transmission rate drastically. Needless
298 to mention that such generic antiviral strategy can significantly reduce the overall burden of seasonal

299 respiratory infection-related epidemics or occasional pandemics caused either by various influenza or
300 coronaviruses.

301 **Materials and Methods**

302 **Chemicals:**

303 Copper sulfate ($\text{CuSO}_4 > 99\%$), Silver nitrate ($\text{AgNO}_3 > 99\%$), Sodium borohydride ($\text{NaBH}_4 > 98\%$), Poly
304 vinyl alcohol ($>99\%$), Sodium hydroxide pellets ($\text{NaOH} > 97\%$) and graphite powder ($>98\%$) were
305 purchased from Sigma-Aldrich.

306

307 **Cells, Viruses and Antibody:** Madin Darby Canine Kidney (MDCK) (CCL-34) cells were maintained in
308 Dulbecco's modified Eagle's medium (DMEM) supplemented with 5% FBS at 37°C and 5% CO_2 along
309 with penicillin and streptomycin antibiotics (Gibco).

310

311 Influenza A virus strains, A/WSN/1933 (H1N1), WSN stably encoding PB2 with a C-terminal FLAG tag
312 (WSN-PB2-FLAG) (Dos Santos Afonso et al. 2005) or PA-2A-Swap-Nluc (PASTN) reporter virus based
313 on the strain A/WSN/33 (H1N1) were used for infecting the cells (Tran et al. 2013). Antibody used
314 includes anti-NP (H16-L10-4R5) (Yewdell et al., 1981).

315

316 **Synthesis of materials:**

317 Initially, the graphene dispersion was prepared using a liquid exfoliation of the graphite powder in
318 Deionized (DI) water (20 mg/300 mL) using an ultrasonic probe sonicator. Probe sonication of frequency
319 30 Hz was used in pulses for 2 hours. Silver (Ag) and Copper (Cu) stock solutions were prepared using
320 4mM AgNO_3 (68 mg/100 mL) and 4 mM CuSO_4 (63.8 mg/100 mL) in DI water medium respectively.
321 Graphene solution (45 mL) was mixed with 15 mL of Cu and Ag stock solution separately by maintaining
322 the pH=12 adjusted through NaOH . 20 mL of 4 mM NaBH_4 (30 mg/200 mL) solution, a strong reducing
323 agent is added drop wise with the Cu-graphene (Cu-Gr), Ag-graphene (Ag-Gr) and Cu-Ag-graphene (Cu-
324 Ag-Gr) mixtures separately and stirred continuously at 40°C .

325 Furthermore, four different concentrations ($1\mu\text{M}$, $5\mu\text{M}$, $10\mu\text{M}$ and $20\mu\text{M}$) of Cu functionalized graphene
326 samples were synthesized for biological process optimization. Three different concentrations (1mM, 5mM
327 and 10mM) of poly vinyl alcohol have been capped as a coating media for the Cu-graphene samples.

328

329 **Material characterizations:**

330 Different phases of the synthesized sample (Cu functionalized graphene) were obtained from the X-ray
331 diffraction (XRD) peaks by using Bruker D8 Advance X-ray diffractometer within a scan range of 2Theta

332 (20) values 7 and 90° with Cu-K α source, maintaining the scan rate of 1° min $^{-1}$. Absorption spectra of Cu-
333 graphene synthesized sample were recorded by a BioTek UV-vis spectrophotometer Epoch 2 microplate
334 within 200 nm to 800 nm wavelength. Raman shifts were measured by using WiTec –alpha 300R confocal
335 microscope at excitation of 532 nm in the wavenumber range of 200 cm $^{-1}$ to 3000 cm $^{-1}$. SEM images were
336 obtained through Zeiss-Merlin EVO 60 scanning electron microscope with Oxford EDS detector.

337

338 **MTT assay:**

339 MDCK cells were seeded in 96 well plates at a density of 15000 cells per well. The cells were treated with
340 Silver (Ag), Graphene (Gr), Copper (Cu) nanoparticles as well as Ag-Gr, Cu-Gr and Ag-Cu-Gr
341 nanocomposites respectively for 24 hours (h) at 37°C in 5% CO $_2$. Cellular cytotoxicity assay was performed
342 according to the manufacturer's protocol. In brief, after 24 h of treatment with the nanoparticle, 100 μ l of
343 MTT reagent (5 mg/ml, SRL) in PBS was added to the cells and incubated for 3 h at 37°C. The medium
344 was removed carefully without disturbing the formazan crystals and 100 μ l of DMSO (Sigma) was added
345 to dissolve the insoluble purple formazan crystals. The absorbance of the suspension was measured at 595
346 nm using Epoch 2 Microplate Reader (BioTek instruments). The percentages of metabolically active cells
347 were compared with the percentage of control cells of the same culture plate as a proxy for cell viability.
348 Cellular cytotoxicity was determined in triplicate and each experiment was repeated three times
349 independently.

350

351 Nano-Luc reporter assay:

352 The Nano-Luc reporter assay was used to determine the luciferase activity as previously mentioned by Tran
353 et al., 2013 (Tran et al. 2013). MDCK cells seeded in a 96 well plate were infected in triplicate with the
354 Nano Luciferase influenza A reporter virus, PASTN. Accordingly, the virus was preincubated with a
355 particular concentration of the nanoparticle/nanocomposite for 30 min or mentioned otherwise. The vehicle
356 control or the nanoparticle/ nanocomposite treated virus was used to infect MDCK cells. The infected cells
357 were harvested at 8hpi and the viral NLuc activity was measured by using Nano-Glo® Luciferase Assay
358 System according to the manufacturer's instructions (Promega) and the luminescence was detected by using
359 a Luminometer (Glomax 20/20, Promega).

360

361 **Plaque assay:**

362 A non-reporter variant of the influenza A/H1N1/WSN/1933 virus stock solutions MOI 0.1 was either
363 preincubated with vehicle control or Cu-Gr nanocomposite (1 μ M and 5 μ M) followed by infection in MDCK
364 cells. At 8hpi, the viral supernatant was collected and used to reinfect MDCK cells and plaque assay was

365 performed to determine the progeny viral titer followed by Matrosovich M, 2006 (Matrosovich et al. 2006).
366 Accordingly, after 1 hr of infection with the virus, cells were overlaid with a media containing a mixture of
367 2X DMEM and 2.4% avicel (1:1 ratio). After 62hrs, the overlay was discarded and the cells were fixed with
368 70% ethanol followed by staining with 2% Crystal violet. Plaques were counted and plaque forming unit
369 (PFU/ml) was calculated to measure the progeny viral titer.

370

371 **Viral entry assay:**

372 MDCK cells grown on coverslips were infected with vehicle control or 5uM Cu-Gr treated virus at a MOI
373 of 5. Viral entry assay was performed according to the protocol followed by Mondal et al., 2017 (Mondal
374 et al. 2017). Virion binding was performed at 4°C for 1hr in presence of 1mM of Cycloheximide, CHX
375 (Sigma). The viral inoculum was washed off with cold PBS to remove unbound virus particles. Thereafter,
376 the prewarmed virus growth media (VGM, containing DMEM, 0.2% bovine serum albumin (BSA), 25 mM
377 HEPES buffer, and 0.5 mg/ml TPCK-trypsin) supplemented with 1mM of CHX was added to the cells and
378 synchronous infection was initiated by shifting cells to 37°C. At 1 hpi, cells were fixed with 3%
379 formaldehyde and permeabilized with 0.1M Glycine/0.1% Triton-X 100 in PBS for 20 min at room
380 temperature. Blocking was performed at 4°C with 3% BSA overnight. NP was detected with anti-NP
381 antibody and Alexa Fluor 555-conjugated donkey anti-mouse IgG antibody (Invitrogen). DAPI (Sigma)
382 was used to stain the nucleus. Cells were imaged using Fluorescent microscope (Leica Microsystems) and
383 image analysis was performed with ImageJ software.

384

385 **Statistics:**

386 Each data is a representative of at least three independent experiments, each experiment was performed in
387 triplicate. Graphs are performed in Microsoft Excel and represented as mean standard deviations (n=3).
388 Results were compared by performing two-tailed Student's t test. Significance is defined as p<0.05 and
389 statistical significance is indicated with an asterisk (*). The *p value < 0.05, **p value < 0.01 ***p value
390 and ***p < 0.001 were considered statistically significant.

391

392 **Acknowledgement:**

393

394 We sincerely thank Prof. Andrew Mehle, University of Wisconsin Madison, for providing the Nano-Luc
395 influenza A reporter viruses. This work was primarily supported by Sponsored Research and Industrial
396 Consultancy (SRIC) IIT Kharagpur. AM would like to thank DBT for Ramalingaswami re-entry fellowship,
397 SERB for Early Career Research Award and MHRD for the "Scheme for Transformational and Advanced
398 Research in Science" for additional financial support.

399
400
401

402 **References**

403 Barani, Zahra et al. 2020. "Thermal Properties of the Binary-Filler Hybrid Composites with Graphene and
404 Copper Nanoparticles." *Advanced Functional Materials* 30(8): 1–11.

405 Chan, George H. et al. 2007. "Plasmonic Properties of Copper Nanoparticles Fabricated by Nanosphere
406 Lithography." *Nano Letters* 7(7): 1947–52.

407 Cioffi, Nicola et al. 2005. "Copper Nanoparticle/Polymer Composites with Antifungal and Bacteriostatic
408 Properties." *Chemistry of Materials* 17(21): 5255–62.

409 Darabdhara, Gitashree et al. 2017. "Cu-Ag Bimetallic Nanoparticles on Reduced Graphene Oxide
410 Nanosheets as Peroxidase Mimic for Glucose and Ascorbic Acid Detection." *Sensors and Actuators,*
411 *B: Chemical* 238: 842–51.

412 Deng, Dunying et al. 2013. "Copper Nanoparticles: Aqueous Phase Synthesis and Conductive Films
413 Fabrication at Low Sintering Temperature." *ACS Applied Materials and Interfaces* 5(9): 3839–46.

414 Deng, Yilin et al. 2016. "In Situ Raman Spectroscopy of Copper and Copper Oxide Surfaces during
415 Electrochemical Oxygen Evolution Reaction: Identification of CuIII Oxides as Catalytically Active
416 Species." *ACS Catalysis* 6(4): 2473–81.

417 Edwards, Rebecca S., and Karl S. Coleman. 2013. "Graphene Synthesis: Relationship to Applications."
418 *Nanoscale* 5(1): 38–51.

419 Eigler, Siegfried, and Andreas Hirsch. 2014. "Chemistry with Graphene and Graphene Oxide -
420 Challenges for Synthetic Chemists." *Angewandte Chemie - International Edition* 53(30): 7720–38.

421 Fehr, Anthony R., and Stanley Perlman. 2015. "Coronaviruses: An Overview of Their Replication and
422 Pathogenesis." *Methods in molecular biology (Clifton, N.J.)* 1282: 1–23.

423 Ferrari, A. C. et al. 2006. "Raman Spectrum of Graphene and Graphene Layers." *Physical Review Letters*
424 97(18): 1–4.

425 Gawande, Manoj B. et al. 2016. "Cu and Cu-Based Nanoparticles: Synthesis and Applications in
426 Catalysis." *Chemical Reviews* 116(6): 3722–3811.

427 Georgakilas, Vasilios et al. 2012. "Functionalization of Graphene: Covalent and Non-Covalent
428 Approach." *Chemical Reviews* 112(11): 6156–6214.

429 Hang, Xiaofeng et al. 2015. "Antiviral Activity of Cuprous Oxide Nanoparticles against Hepatitis C Virus
430 in Vitro." *Journal of Virological Methods* 222: 150–57.
431 <http://dx.doi.org/10.1016/j.jviromet.2015.06.010>.

432 Hu, Yanjie et al. 2013. "Scalable Preparation of Ultrathin Silica-Coated Ag Nanoparticles for SERS

433 Application.” *ACS Applied Materials and Interfaces* 5(21): 10643–49.

434 Jane Flint, Vincent R, Glen F Rall and Anna Marie with Lynn W Enquist. 2015. *Principles of Virology*,
435 *4th Edition*.

436 Jin, Rongchao, Justin E. Jureller, Hee Y. Kim, and Norbert F. Scherer. 2005. “Correlating Second
437 Harmonic Optical Responses of Single Ag Nanoparticles with Morphology.” *Journal of the*
438 *American Chemical Society* 127(36): 12482–83.

439 Johnson, Niall P.A.S., and Juergen Mueller. 2002. “Updating the Accounts: Global Mortality of the 1918–
440 1920 ‘Spanish’ Influenza Pandemic.” *Bulletin of the history of medicine* 76(1): 105–15.

441 Karahan, Hüseyin Enis et al. 2018. “Graphene Materials in Antimicrobial Nanomedicine: Current Status
442 and Future Perspectives.” *Advanced Healthcare Materials* 7(13): 1–18.

443 Kim, Un Jeong et al. 2018. “Anomalous K-Point Phonons in Noble Metal/Graphene Heterostructure
444 Activated by Localized Surface Plasmon Resonance.” *ACS Nano* 12(12): 12733–40.

445 Koven, S. 2020. “Engla, Journal - 2010 - New Engla Nd Journal.” *New England Journal of Medicine*: 1–
446 2.

447 Landrigan, Philip J. et al. 2018. “The Lancet Commission on Pollution and Health.” *The Lancet*
448 391(10119): 462–512.

449 Letko, Michael, Andrea Marzi, and Vincent Munster. 2020. “Functional Assessment of Cell Entry and
450 Receptor Usage for SARS-CoV-2 and Other Lineage B Betacoronaviruses.” *Nature Microbiology*
451 5(4): 562–69.

452 Lin, Leon Chien Wei et al. 2019. “Viromimetic STING Agonist-Loaded Hollow Polymeric Nanoparticles
453 for Safe and Effective Vaccination against Middle East Respiratory Syndrome Coronavirus.”
454 *Advanced Functional Materials* 29(28): 1–15.

455 Ma, Jizhen et al. 2011. “Preparation, Characterization and Antibacterial Properties of Silver-Modified
456 Graphene Oxide.” *Journal of Materials Chemistry* 21(10): 3350–52.

457 Matrosovich, Mikhail, Tatyana Matrosovich, Wolfgang Garten, and Hans Dieter Klenk. 2006. “New
458 Low-Viscosity Overlay Medium for Viral Plaque Assays.” *Virology Journal* 3: 1–7.

459 Minoshima, Masafumi et al. 2016. “Comparison of the Antiviral Effect of Solid-State Copper and Silver
460 Compounds.” *Journal of Hazardous Materials* 312: 1–7.

461 Mohammed, Hiba et al. 2020. “Antimicrobial Mechanisms and Effectiveness of Graphene and Graphene-
462 Functionalized Biomaterials. A Scope Review.” *Frontiers in Bioengineering and Biotechnology*
463 8(May).

464 Mondal, Arindam et al. 2017. “Influenza Virus Recruits Host Protein Kinase C to Control Assembly and
465 Activity of Its Replication Machinery.” *eLife* 6: 1–23.

466 Neeltje van Doremale, PhD et al. 2020. “Aerosol and Surface Stability of SARS-CoV-2 as Compared

467 with SARS-CoV-1.” *New England Journal of Medicine*: 0–2.

468 Novoselov, K. S. et al. 2012. “A Roadmap for Graphene.” *Nature* 490(7419): 192–200.

469 <http://dx.doi.org/10.1038/nature11458>.

470 Palmieri, V., and M. Papi. 2020. “Can Graphene Take Part in the Fight against COVID-19?” *Nano Today*

471 33: 100883.

472 Park, Se Jin et al. 2020. “Discovery of Direct-Acting Antiviral Agents with a Graphene-Based

473 Fluorescent Nanosensor.” *Science Advances* 6(22): 1–12.

474 Patterson, David, and Gerald Pyle. 2019. “The Geography and Mortality of the 1918 Influenza

475 Pandemic.” *Bulletin of the History of Medicine* 65(1): 4–21.

476 Perdikaki, Anna et al. 2018. “Ion-Based Metal/Graphene Antibacterial Agents Comprising Mono-Ionic

477 and Bi-Ionic Silver and Copper Species.” *Langmuir* 34(37): 11156–66.

478 Ramakrishnan, S. et al. 2015. “One-Step Synthesis of Pt-Decorated Graphene-Carbon Nanotubes for the

479 Electrochemical Sensing of Dopamine, Uric Acid and Ascorbic Acid.” *Analytical Methods* 7(2):

480 779–86.

481 Ruparelia, Jayesh P., Arup Kumar Chatterjee, Siddhartha P. Duttagupta, and Suparna Mukherji. 2008.

482 “Strain Specificity in Antimicrobial Activity of Silver and Copper Nanoparticles.” *Acta*

483 *Biomaterialia* 4(3): 707–16.

484 Dos Santos Afonso, Emmanuel et al. 2005. “The Generation of Recombinant Influenza A Viruses

485 Expressing a PB2 Fusion Protein Requires the Conservation of a Packaging Signal Overlapping the

486 Coding and Noncoding Regions at the 5' End of the PB2 Segment.” *Virology* 341(1): 34–46.

487 Saunders-Hastings, Patrick R., and Daniel Krewski. 2016. “Reviewing the History of Pandemic

488 Influenza: Understanding Patterns of Emergence and Transmission.” *Pathogens* 5(4).

489 Shen, Jianfeng et al. 2010. “Facile Synthesis and Application of Ag-Chemically Converted Graphene

490 Nanocomposite.” *Nano Research* 3(5): 339–49.

491 Sunada, Kayano, Masafumi Minoshima, and Kazuhito Hashimoto. 2012. “Highly Efficient Antiviral and

492 Antibacterial Activities of Solid-State Cuprous Compounds.” *Journal of Hazardous Materials* 235–

493 236: 265–70. <http://dx.doi.org/10.1016/j.jhazmat.2012.07.052>.

494 Taubenberger, Jeffery K., and David M. Morens. 2006. “1918 Influenza: The Mother of All Pandemics.”

495 *Emerging Infectious Diseases* 12(1): 15–22.

496 Ting Du., et al. 2018. “Antiviral Activity of Graphene Oxide–Silver Nanocomposites _2018.Pdf.”

497 Tran, V., L. A. Moser, D. S. Poole, and A. Mehle. 2013. “Highly Sensitive Real-Time In Vivo Imaging of

498 an Influenza Reporter Virus Reveals Dynamics of Replication and Spread.” *Journal of Virology*

499 87(24): 13321–29.

500 Vasickova, P, I Pavlik, M Verani, and A Carducci. 2010. “Issues Concerning Survival of Viruses on

501 Surfaces.” *Food and Environmental Virology* 2(1): 24–34.

502 Vinothini, Kandasamy, and Mariappan Rajan. 2017. “Investigation on the Use of Graphene as a Unique
503 Drug Delivery Platform for Dissimilar Anticancer Drugs.” *Progress in Bioscience and*
504 *Bioengineering* 1(1): 11–17.

505 De Wit, Emmie, Neeltje Van Doremalen, Darryl Falzarano, and Vincent J. Munster. 2016. “SARS and
506 MERS: Recent Insights into Emerging Coronaviruses.” *Nature Reviews Microbiology* 14(8): 523–
507 34.

508 World Health Organization. 2018. “The Top 10 Causes of Death.” *World Health Organization*.

509 Wu, Jiang Bin et al. 2018. “Raman Spectroscopy of Graphene-Based Materials and Its Applications in
510 Related Devices.” *Chemical Society Reviews* 47(5): 1822–73.

511 Wu, Yuntao et al. 2020. “SARS-CoV-2 Is an Appropriate Name for the New Coronavirus.” *The Lancet*
512 395(10228): 949–50.

513 Yao, Wei Tang et al. 2005. “Formation of Uniform CuO Nanorods by Spontaneous Aggregation:
514 Selective Synthesis of CuO, Cu₂O, and Cu Nanoparticles by a Solid-Liquid Phase Arc Discharge
515 Process.” *Journal of Physical Chemistry B* 109(29): 14011–16.

516 Ye, Shiyi et al. 2015. “Antiviral Activity of Graphene Oxide: How Sharp Edged Structure and Charge
517 Matter.” *ACS Applied Materials and Interfaces* 7(38): 21578–79.

518 Zhang, Zhuanfang et al. 2020. “Facile Hydrothermal Synthesis of CuO-Cu₂O/GO Nanocomposites for
519 the Photocatalytic Degradation of Organic Dye and Tetracycline Pollutants.” *New Journal of*
520 *Chemistry* 44(16): 6420–27.

521 Ziem, Benjamin et al. 2016. “Highly Efficient Multivalent 2D Nanosystems for Inhibition of
522 Orthopoxvirus Particles.” *Advanced Healthcare Materials* 5(22): 2922–30.

523

524

525 **Figure legends**

526 **Figure 1. Different nanoparticles and their nanocomposites.** (A) Digital photographs of all the
527 synthesized nanoparticle and nanocomposite samples. (B) Schematic representation of the Cu and Ag
528 nanoparticles embedded two dimensional graphene sheets. (C-D) UV-Vis absorption spectra of synthesized
529 nanoparticles and their composites.

530 **Figure 2. Nanoparticles and nanocomposites shows minimal cytotoxicity.** MDCK cells were either
531 treated with vehicle control or different concentrations (0.5, 1, 5 μ M) of the Ag, Cu and Gr nanoparticles
532 or Ag-Gr, Cu-Gr and Ag-Cu-Gr nanocomposites for 24 h and their cytotoxicity were determined by MTT
533 assay. Cellular cytotoxicity was determined in triplicate and each experiment was repeated three times.
534 Data are presented as means \pm standard deviations (SD) (n=3).

535

536 **Figure 3. Screening of different the nanoparticles/ nanocomposites for antiviral activity using Nano-**
537 **Luciferase influenza A reporter.** (A) MDCK cells were infected with different amounts (0.01-0.1) of
538 Nano-Luciferase Influenza A reporter virus and the reporter activity was measured using Nano glo reporter
539 assay (Promega). To demonstrate the relationship between the MOI and luciferase activity (arbitrary unit)
540 was plotted as a function of MOI. (B) To test the antiviral activity, the Influenza A reporter virus was
541 pretreated with the 5uM colloidal suspensions of each of the materials for 30 minutes at RT and followed
542 by infection of MDCK cells at MOI of 0.1as diagrammed. (C) Luciferase activity of the nanoparticle/
543 nanocomposite treated sets were measured at 8 hpi and plotted as a relative percentage of the vehicle treated
544 set. For all experiments, data are mean of n=3± standard deviation (*, P< 0.05; n=3 ± sd).

545

546 **Figure 4. Material characterization of the Cu-Gr nanocomposite.** (A) Raman spectrum of Cu-Gr
547 nanocomposites. Inset shows optical microscopy image of the composite and Raman spectrum of Cu_xO.
548 (B) XRD spectrum of composites sample confirming the presence of CuO, Cu₂O, and Graphene.

549

550 **Figure 5. Prior incubation with Cu-Gr nanocomposite severely impacts the infectivity of influenza A**
551 **virus.** (A) A time kinetics experiment was performed by treating Influenza A reporter virus with 5uM
552 colloidal suspensions of Cu-Gr for 15, 30, 45 and 60 min at RT and followed by infection of MDCK cells
553 at MOI 0.1. Absolute luciferase activity values w.r.t viral gene expression for the vehicle and Cu-Gr treated
554 sets are represented by black and grey bars respectively. (B) MDCK cells were infected with Influenza A
555 reporter virus pretreated with vehicle or with different concentrations of the Cu-Gr composite (50nM,
556 100nM, 500nM, 1uM, 2uM and 5uM respectively). Viral gene expression was monitored using luciferase
557 activity assay. Data were normalized to vehicle control sets for each nanoparticle. (C, D) A non-reporter
558 A/H1N1/WSN/1933 influenza virus was either treated with Cu-Gr composite (1uM and 5uM) or with
559 vehicle control prior to infecting MDCK cells. Plaque assay was performed to measure the titer of the
560 progeny virus particles harvested at 8hpi. Percentage reduction in viral titers and actual PFUs for all
561 experiments are represented. For all experiments, data are mean of n=3± standard deviation (*, P< 0.05;
562 n=3 ± sd).

562

563 **Figure 6. Cu-Gr interferes with the entry of Influenza A virus inside the cells.** (A) Schematic depiction
564 of Entry assay: MDCK cells were infected with influenza A virus either pretreated with 5uM Cu-Gr or with
565 vehicle control. Synchronous infection was carried out by incubating the virus inoculum with the cell
566 monolayer at 4⁰C for one hour, followed by adding the virus growth media (VGM) supplemented with
567 cycloheximide and prewarmed at 37⁰C. Cells were incubated further for one hour before processing them
568 for imaging (B) Intracellular localization of viral NPs in control and Cu-Gr treated sets were determined by
569 staining with anti NP antibody and Alexa Fluor 555 (red). DAPI was used to stain the nucleus (Blue). (C)

570 Percentage of NP positive cells in control and in treated sets were analyzed using image J software and
571 depicted by bar diagram. For all experiments, data are mean of $n=5 \pm$ standard deviation (*, $P < 0.05$).

572 **Figure 7. PVA based Cu-Gr nanocomposite coating shows strong antiviral activity.** Different wells of
573 a 48 well plate was coated with coating solutions having different concentrations of Cu-Gr composite (1uM,
574 5 uM, 10 uM and 20 uM) and polyvinyl alcohol (PVA) (1mM, 5mM and 10mM). Nano Luciferase-
575 Influenza A virus (MOI 0.1) were inoculated in these wells and incubated for 30 minutes. Post treatment,
576 MDCK cells were infected with the viral inoculum recovered from the coated wells and luciferase activity
577 was determined at 8 hpi using Nano-Glo reporter assay (Promega). Luciferase activity of each set was
578 plotted as a relative percentage of the vehicle treated set. Each data was represented in triplicate and each
579 experiment was repeated three times. Data are presented as means \pm standard deviations (SD) ($n=3$) (*, $P <$
580 0.05).

581

582 **Figure 8. PVA based Cu-Gr nanocomposite can be used to generate a highly transparent antiviral
583 coating of the cell phone screen.** (A) Schematic diagram of the deep coating method of tempered glass
584 unit with the PVA based Cu-Gr nanocomposite. (B) Transparency of dip coated tempered mobile screen.
585 (C) Transmittance spectrum of the coated sample. (D) SEM image of Cu-Graphene composites sample.
586 Right panel shows the color mapping of all elements. (E) EDX spectra of composites sample, confirm the
587 presence of Cu, C and O atoms. (F) Schematic representation of the composite structure.
588

589

590

591

592

593

594

595

596

597

598

599

600

601

Figure 1

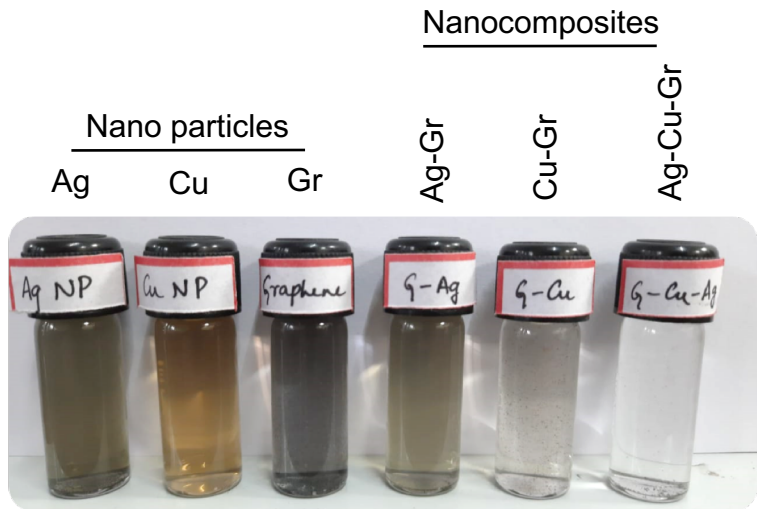
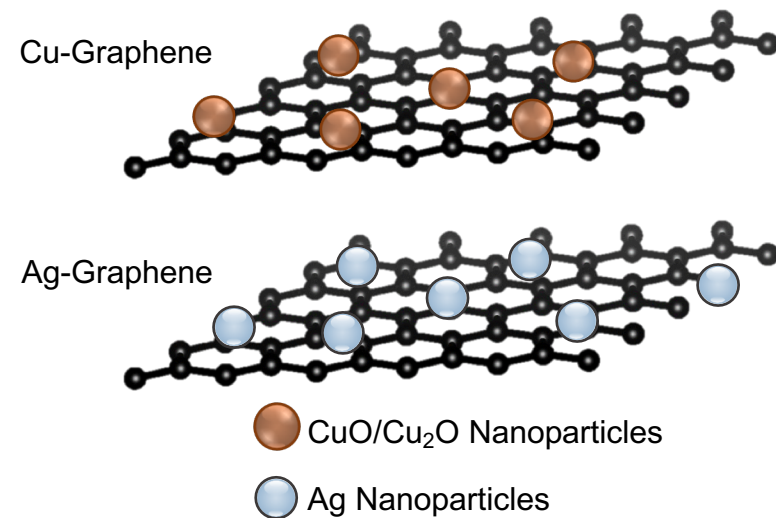
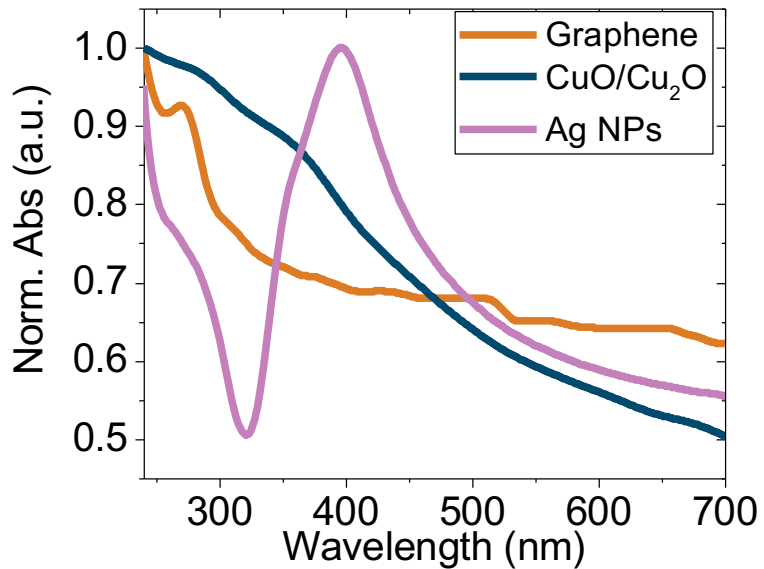
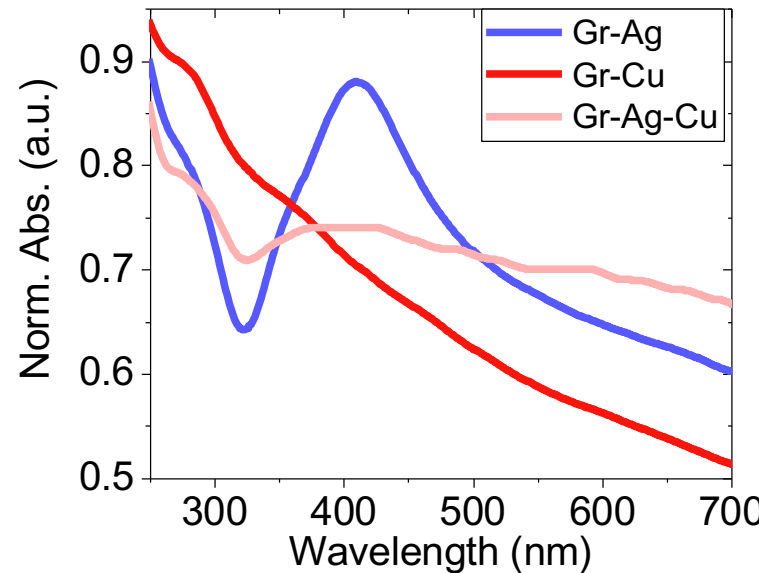
A**B****C****D**

Figure 2

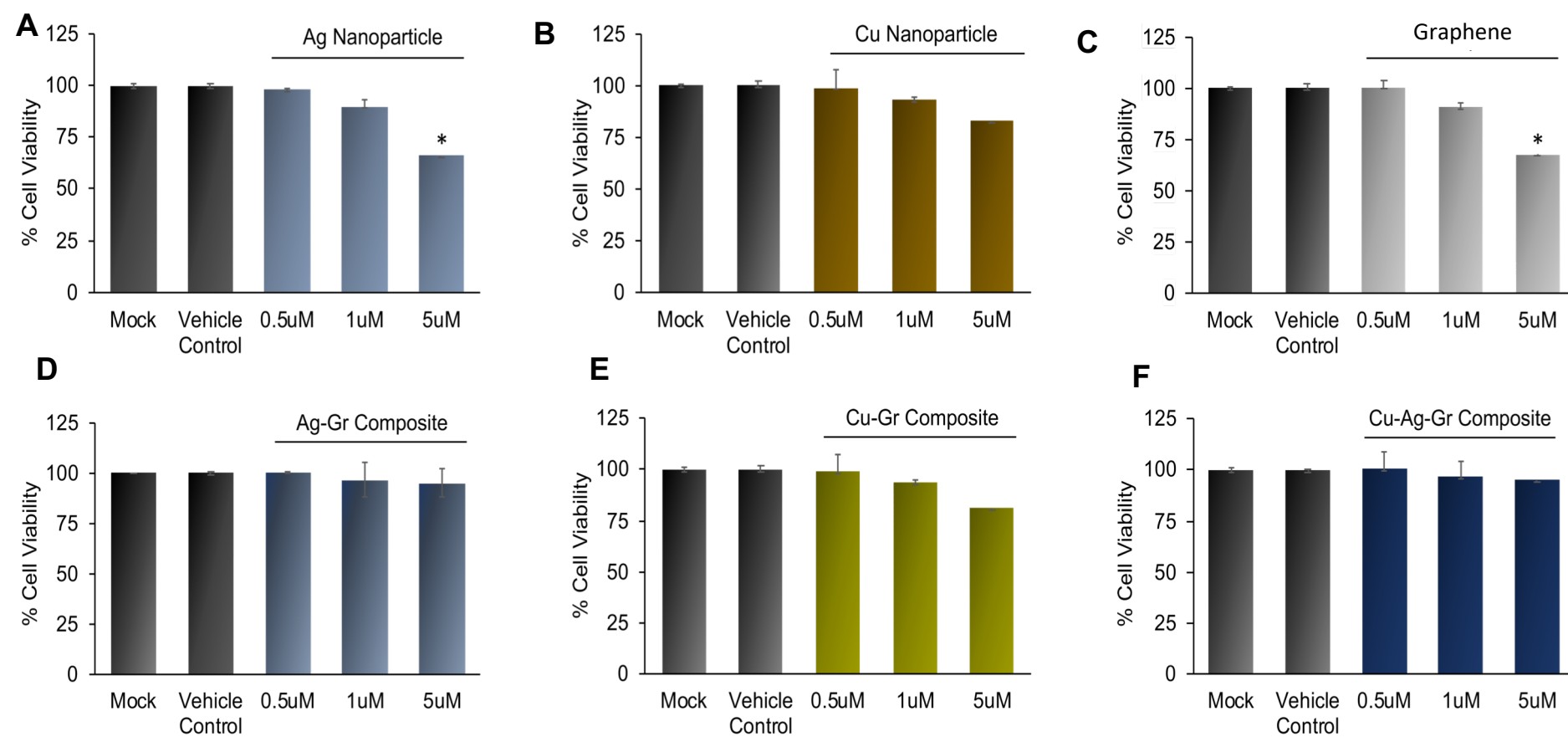


Figure 3

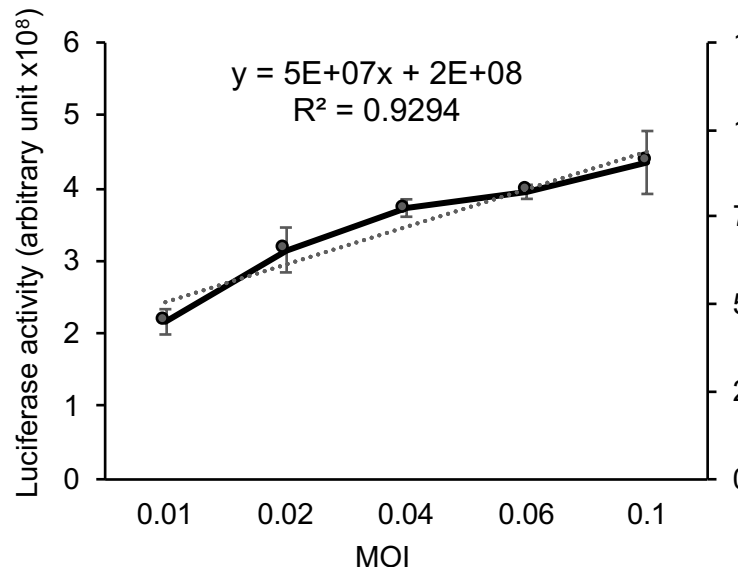
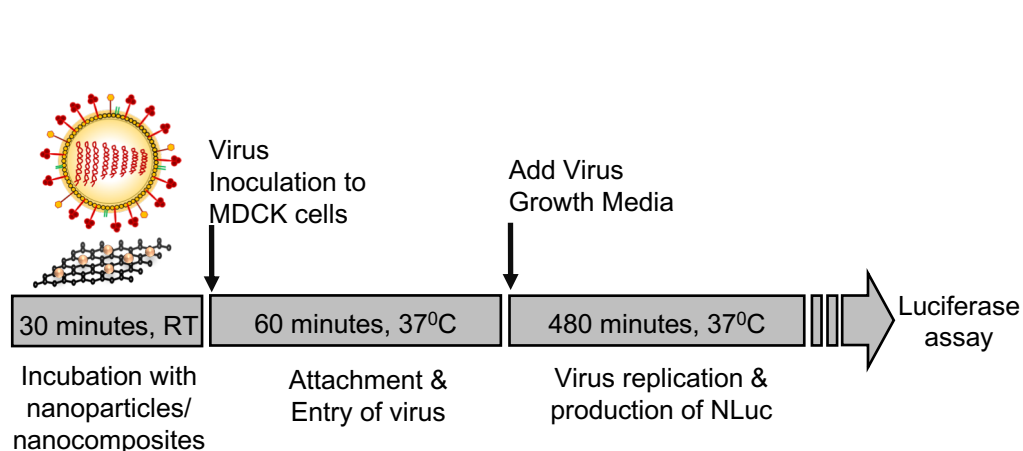
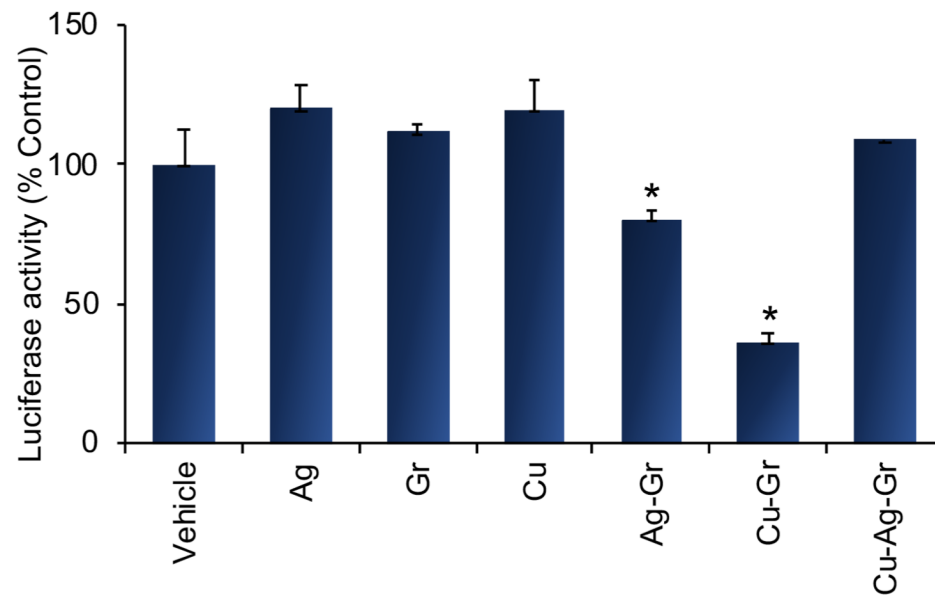
A**B****C**

Figure 4

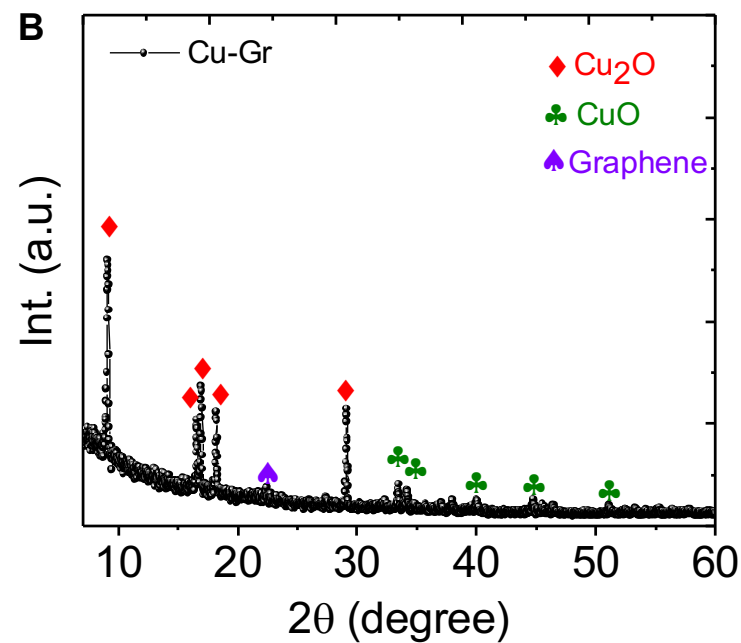
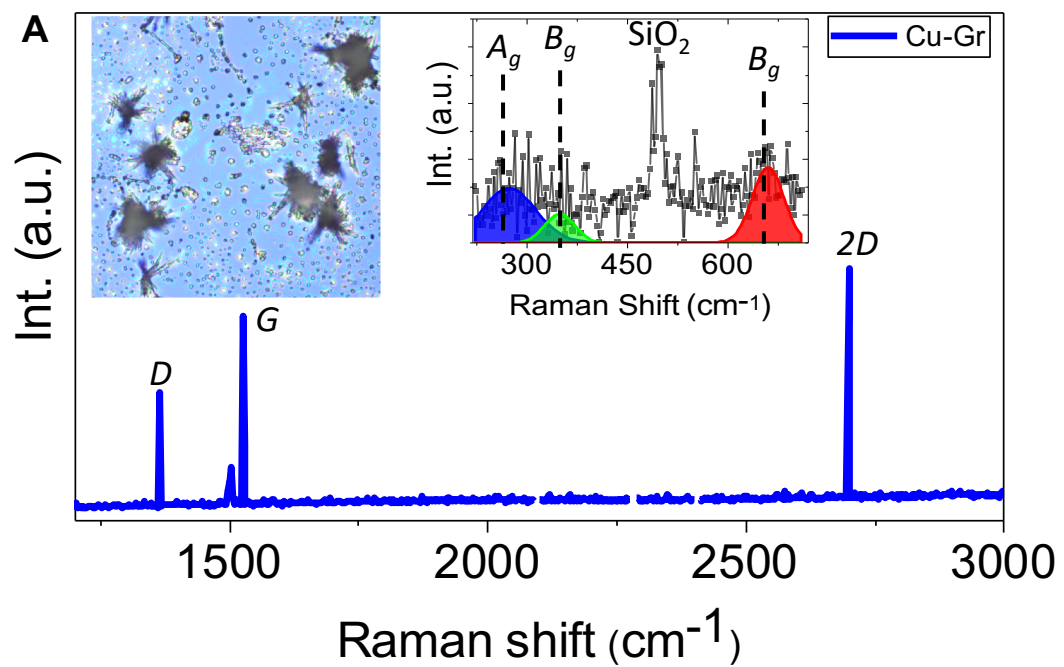
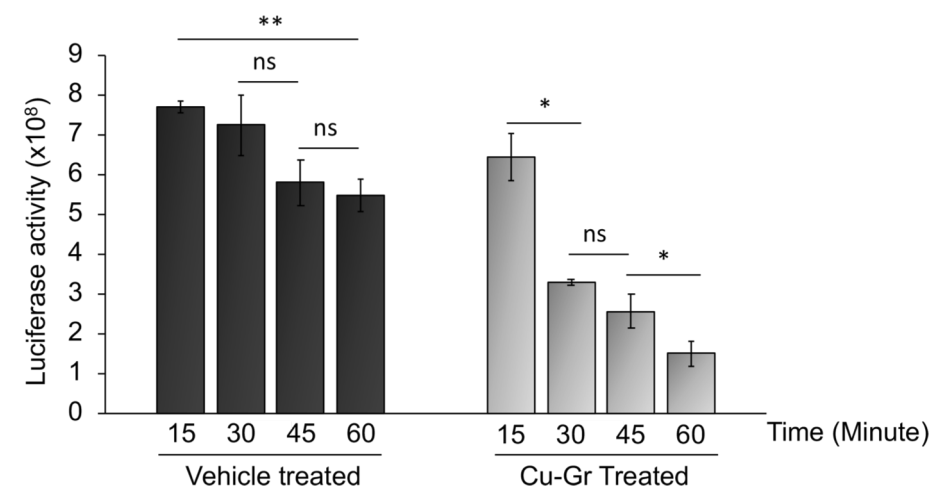
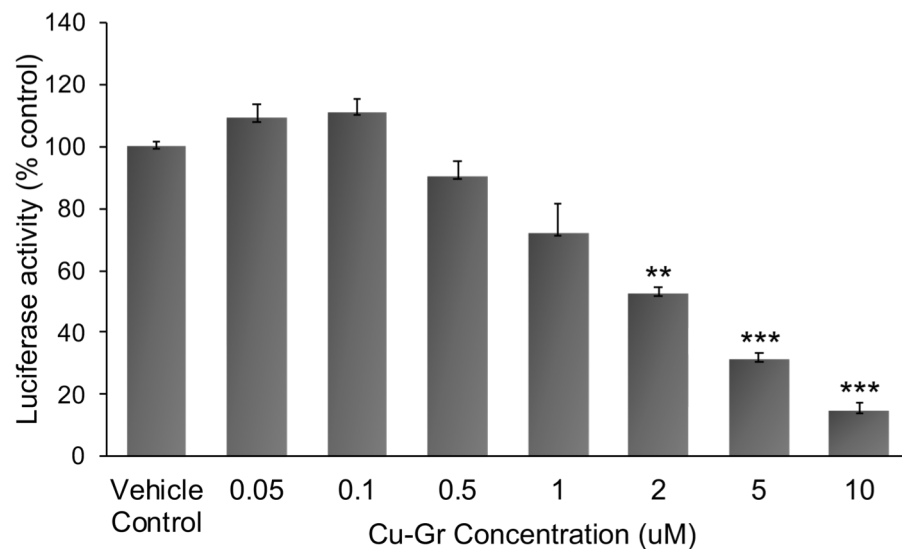
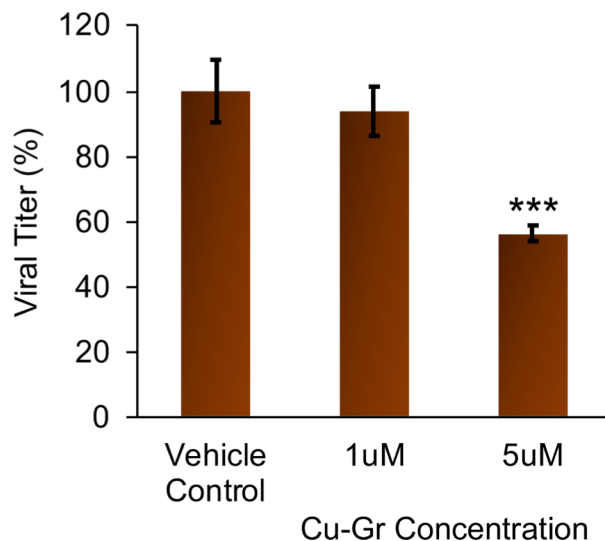


Figure 5**A****B****C****D**

	Viral titer (Pfu/ml)		
	Replicate-1	Replicate-2	Replicate-3
Vehicle Control	57000	50000	55000
Cu-Gr 1uM	54000	48000	50000
Cu-Gr 5uM	29000	31000	31000

Figure 6

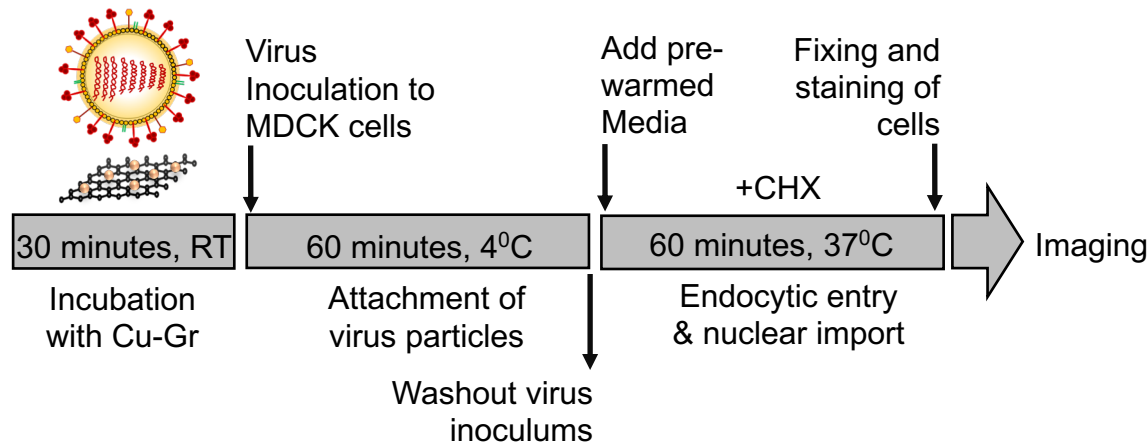
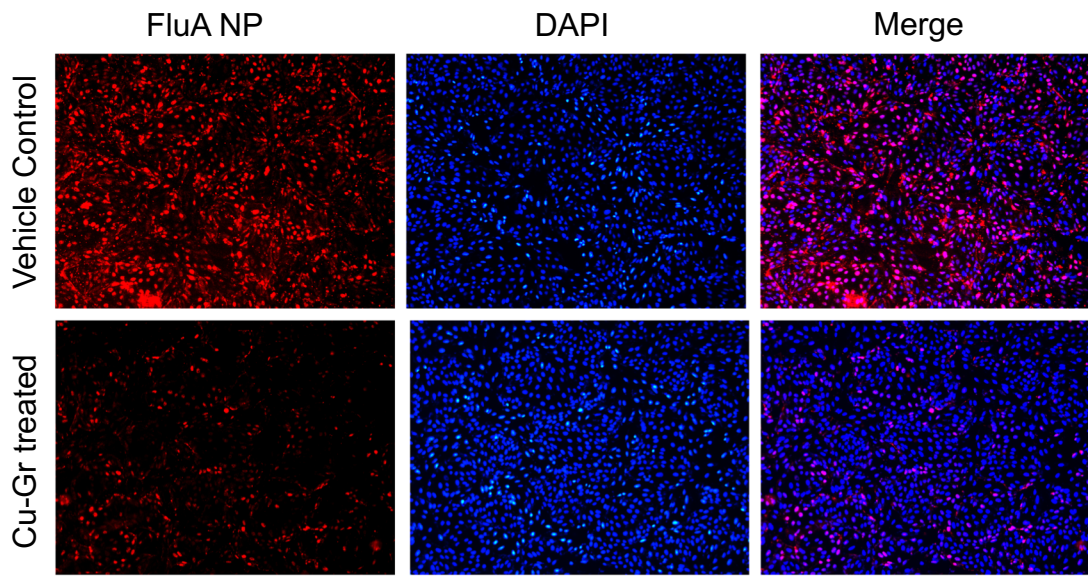
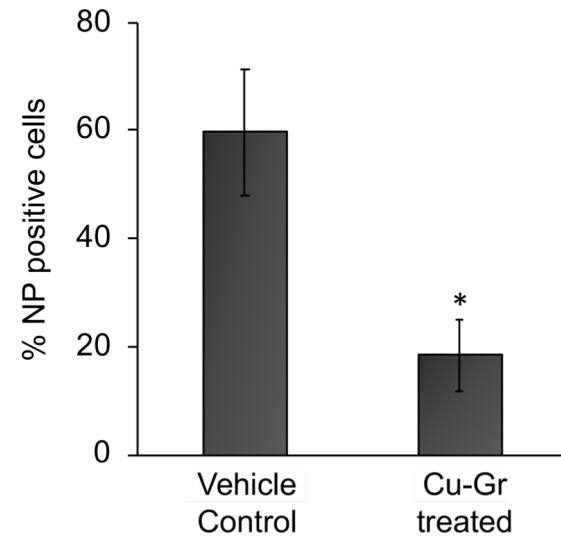
A**B****C**

Figure 7

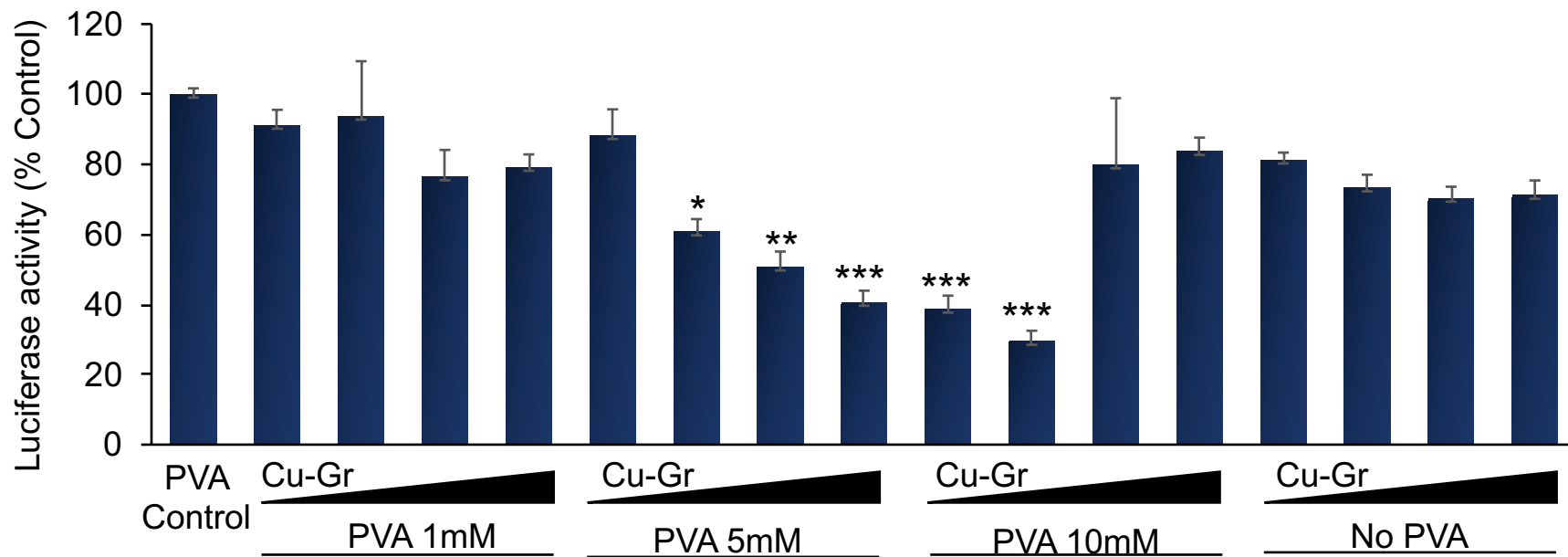
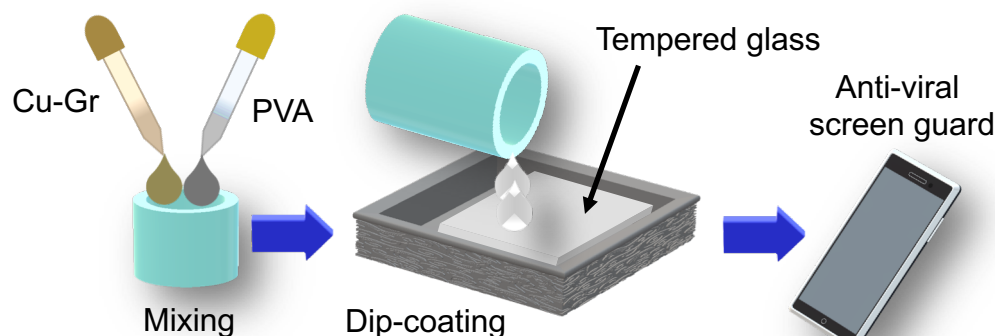
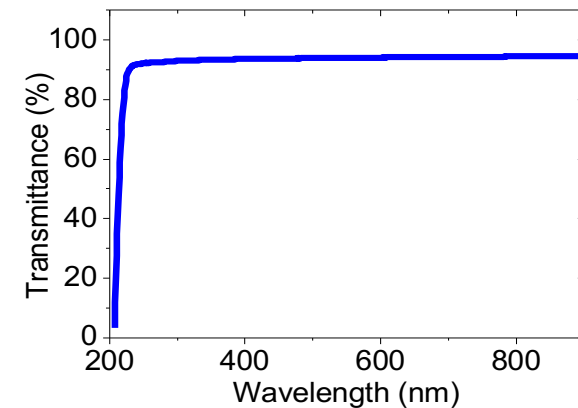
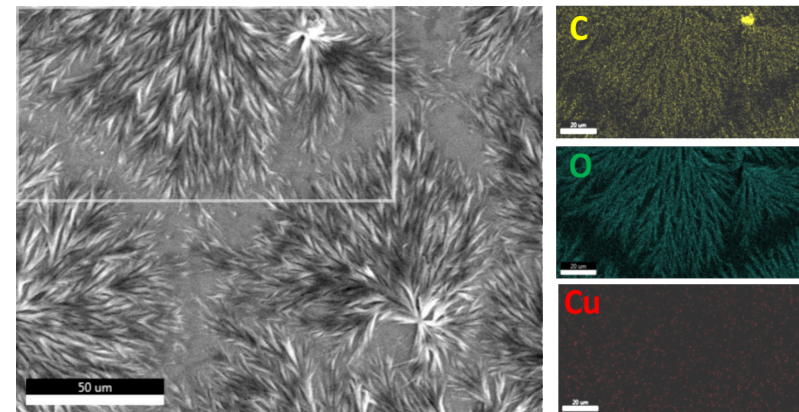
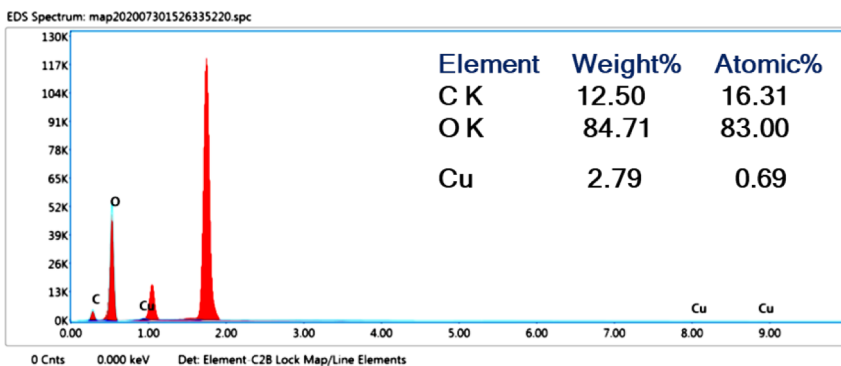


Figure 8

A**C****B****D****E****F**